Flexible Adaptations in the Structure of the tRNA-Modifying Enzyme tRNA – Guanine Transglycosylase and Their Implications for Substrate Selectivity, Reaction Mechanism and Structure-Based Drug Design

Ruth Brenk, Milton T. Stubbs, Andreas Heine, Klaus Reuter, and Gerhard Klebe*[a]

The enzyme tRNA – guanine transglycosylase (TGT, EC 2.4.2.29) catalyses a base-exchange reaction that leads to anticodon modifications of certain tRNAs. The TGT enzymes of the eubacteria Zymomonas mobilis *(*Z. mobilis *TGT) and* Escherichia coli *(*E. coli *TGT) show a different behaviour in the presence of competitive inhibitors. The active sites of both enzymes are identical apart from a single conservative amino acid exchange, namely Tyr106 of* Z. mobilis *TGT is replaced by a Phe in* E. coli *TGT. Although Tyr106 is, in contrast to Phe106, hydrogen bonded in the ligand-free structure, we can show by a mutational study of TGT(Y106F) that this is not the reason for the different responses upon competition. The TGT enzymes of various species differ in their substrate selectivity. Depending on the applied pH conditions and/or induced by ligand binding, a peptide-bond flip modulates the recognition properties of the substrate binding site, which changes between donor and acceptor functionality. Furthermore interstitial water molecules play an important role in these adaptations of the pocket. The flip of the peptide bond is further stabilised by a glutamate residue that operates as general acid/base. An active-site aspartate residue, presumed to operate as a nucleophile through covalent bonding during the base-exchange reaction, shows different conformations depending on the nature of the bound ligand. The induced-fit adaptations observed in the various TGT complex structures by multiple crystal-structure analyses are in agreement with the functional properties of the enzyme. In consequence, full understanding of this plasticity can be exploited for drug design.*

Introduction

The tRNA-modifying enzyme tRNA – guanine transglycosylase (TGT, EC 2.4.2.29) is involved in the post-transcriptional modification of tRNAs.[1] TGT catalyses a base-exchange reaction that proceeds through a covalently bound intermediate (Figure 1). During this reaction, a glycosidic bond of a specific guanosine unit is cleaved without breaking the phosphodiester backbone and a modified base is incorporated into the tRNA in a process that follows an associative mechanism.[2, 3] In prokaryotes and eukaryotes, the activity of TGT finally leads to tRNAs containing the hypermodified base queuine (Q, 7-(((4,5-*cis*-dihydroxy-2-cylcopenten-1-yl)amino)methyl)-7-deazaguanine, Figures 2 and 3).[1, 4] However, in archaebacteria, through TGT-catalysis and subsequent enzymatic reactions tRNAs incorporating the related base archaeosine (G*, 7-formamidino-7-deazaguanine, Figure 3) are formed.[5] Accordingly, the TGTs of the three kingdoms of life differ in substrate selectivity with respect to the recognised base and tRNA.

Prokaryotic TGT catalyses the exchange of the queuine precursor $preQ_1$ (7-(aminomethyl)-7-deazaguanine, Figure 3) against the guanine residue in position 34 (the "wobble position") of tRNAs exhibiting the anticodon sequence GUN ($tRNA^{Asp,Asn,His,Tyr}$).[1] In the following reaction steps, the $preQ_1$, already incorporated into the tRNA, is first transformed into an epoxy-queuine (tRNA-oQueuosine) by QueA and finally reduced to queuine (tRNA-Queuosine) by an as yet unknown enzyme (Figure 2). The substrate $preQ_1$ is probably derived from guanine by an independent biochemical pathway. In contrast, eukaryotic TGTs directly incorporate queuine into tRNAs with the anticodon sequence GUN.[4] Since the final product of both biological pathways is queuosine, these enzymes are also referred to as queuosine TGTs (QueTGT).

Archaebacterial TGT uses a different base as well as a set of different tRNAs as natural substrates.[5] These enzymes catalyse the exchange of guanine in position 15 of the D-loop of various

[a] *Prof. Dr. G. Klebe, Dr. R. Brenk, Prof. Dr. M. T. Stubbs,[+] Dr. A. Heine, Priv. Doz. Dr. K. Reuter*
Institut für Pharmazeutische Chemie
Philipps-Universität Marburg
Marbacher Weg 6, 35032 Marburg (Germany)
Fax: (+49) 6421 2828994
E-mail: klebe@mailer.uni-marburg.de

[+] *Present address:*
Institut für Biotechnologie, Martin-Luther-Universität Halle-Wittenberg
Kurt-Mothes-Strasse 3, 06120 Halle (Saale) (Germany)

  DOI: 10.1002/cbic.200300644

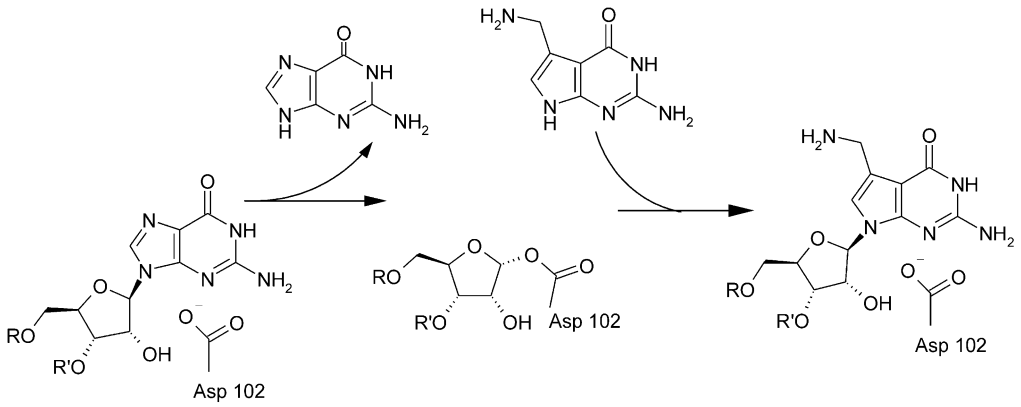

Figure 1. *Catalytic mechanism of prokaryotic TGT. The enzyme catalyses a base-exchange of guanine in the wobble position of certain tRNAs against $preQ_1$. The reaction follows an associative mechanism.*

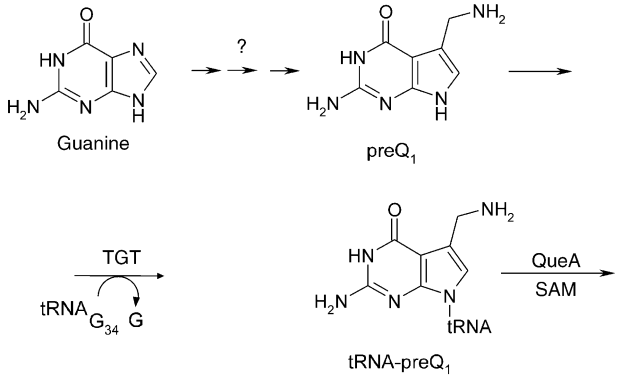

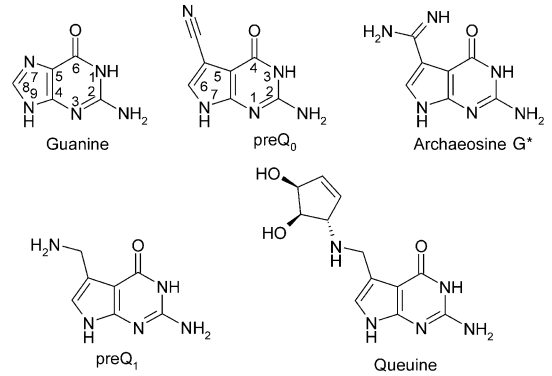

Figure 3. *Chemical structure of guanine and derivatives of 7-deaza-guanine.*

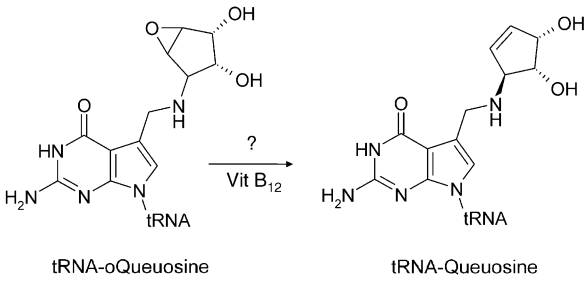

Figure 2. *Biosynthesis of queuosine in prokaryotes. In eukaryotes, queuine is directly incorporated into tRNA whereas archaebacterial TGT incorporates $preQ_0$ which is then further modified to archaeosine (see Figure 3). QueA = S-adenosyl-methionin-tRNA-ribosyltransferase-isomerase, SAM = S-adenosyl-methionine.*

tRNAs against $preQ_0$ (7-cyano-7-deazaguanine, Figure 3) which is subsequently transformed to archaeosine. Since archaeosine is the final product of this pathway, the corresponding enzymes are called archaeosine TGTs (ArcTGT).

Beside their natural substrates, the TGTs of the different kingdoms also accept additional bases, with eukaryotic TGT showing the lowest selectivity (Table 1).[4–6] This enzyme accepts the physiological substrates of all the other TGTs, including guanine. Prokaryotic TGT accepts $preQ_0$ and guanine in addition to its natural substrate $preQ_1$. The most pronounced selectivity is established by archaebacterial TGT, which only accepts its natural substrate $preQ_0$ and guanine.

Table 1. *Substrate selectivity of TGTs of the different kingdoms of life.[a]*

Enzyme	Guanine[b]	$preQ_0$[b]	$preQ_1$[b]	Queuine[b]
archaebacterial TGT	x	x	-	-
prokaryotic TGT	x	x	x	-
eukaryotic TGT	x	x	x	x

[a] x = accepted as substrate; - = not accepted. [b] For chemical formulae see Figure 3.

The crystal structure of *Z. mobilis* TGT has been determined from the class of prokaryotic TGTs.[7] This enzyme belongs to the family of $(\alpha/\beta)_8$-barrels (TIM-barrels, Figure 4a). Differing from the usual fold, where the eight α/β units of the barrel follow one contiguous stretch, several additional secondary structural elements are inserted in the *Z. mobilis* TGT between the α/β units. At the N-terminus, a three-stranded antiparallel β sheet closes up the N-terminal side of the barrel. The barrel makes up the central part of the protein. A C-terminal subdomain is attached to the barrel and contains a structural zinc ion coordinated by the four amino acids Cys318, Cys320, Cys323 and His349. The zinc binding site and the barrel are connected

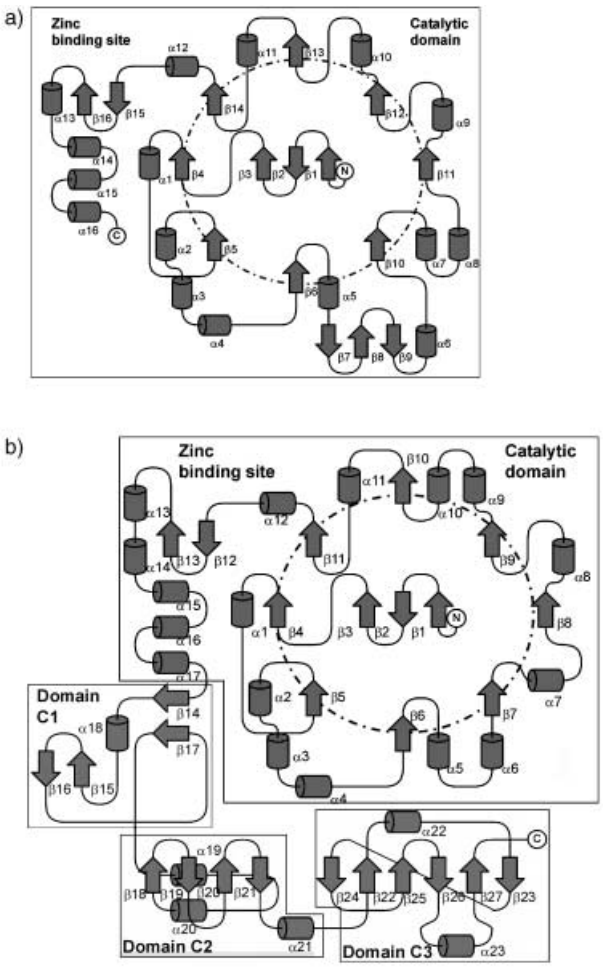

Figure 4. *Schematic folding patterns of prokaryotic (a) and archaebacterial TGT (b). Both enzymes display a $(\alpha/\beta)_8$-barrel as central part but show different inserted elements. In addition to the catalytic domain, archaebacterial TGT has three further domains which may be responsible for its different tRNA recognition characteristics.*

by helix α12. This helix is the terminal one of the $(\alpha/\beta)_8$ motif and comprises the basic amino acids Arg286 and Arg289 which are assumed to be involved in tRNA binding. The active site is located at the C-terminal face of the barrel. In the absence of a ligand, the side chain of Tyr106 closes up the active site by forming hydrogen-bonds to Asp156 and Gln203 (see Figure 5 d). After substrate binding, these bonds are disrupted and the base to be exchanged intercalates between the hydrophobic amino acids Met260 and Tyr106 (Figure 5 a). The substrate is specifically recognised by hydrogen bonds to Asp156, Gly230, Gln203 and Leu231. Except for the replacement of Tyr106 by Phe, these amino acids are highly conserved among prokaryotic TGTs.[8] To date, no crystal structure of *Z. mobilis* TGT in complex with tRNA has been determined. It is assumed that the tRNA interacts with the positively charged zinc binding subdomain and that guanine 34 binds into the same pocket that is occupied by $preQ_1$ in the binding complex.[3, 7]

From the class of archaebacterial TGTs, the crystal structure of ArcTGT from *Pyrococcus horikoshii* has been determined.[9] The N-terminal end of ArcTGT is homologous to prokaryotic QueTGT,

Figure 5. *a) Binding mode of $preQ_1$ complexed with prokaryotic TGT. The terminal amino group of the ligand donates a hydrogen atom to the carbonyl group of Leu231. (Coordinates taken from ref. [7].) b) Binding mode of $preQ_0$ complexed with ArcTGT. The cyano group of the ligand is hydrogen bonded to Val198. (Coordinates taken from ref. [9].) c) Crystal structure of* Z. mobilis *TGT(Y106F) in complex with $preQ_1$ at 1.90 Å resolution. The position of the substrate which has been omitted during refinement is very well defined in the $|F_o|-|F_c|$ electron-density map (contoured at 2.5 σ). d) Crystal structure of* Z. mobilis *TGT(Y106F) (yellow) at 1.95 Å resolution superimposed with the uncomplexed structure of the wild-type enzyme (cyan) and the structure of TGT(Y106F)·$preQ_1$ (grey). The shape of the $|F_o|-|F_c|$ electron-density map (contoured at 2.5 σ) after the first refinement (Tyr106 was replaced by Ala) clearly shows, that contrary to Tyr106 the Phe106 residue in the uncomplexed structure adopts the substrate binding conformation. (Coordinates for the wild-type structures taken from ref. [7].) e) Domino effect initiated by the rotation of Asp102, the arrows indicate the dynamic motion of the various residues. The structure of TGT·$preQ_0$ (grey), crystallised at pH 5.5, is superimposed with that of TGT·**2** (yellow), soaked at pH 8.5. (Coordinates for TGT·2 taken from ref. [24].) f) $|F_o|-|F_c|$ electron-density map (contoured at 1.0 σ) for the ligand **4** and Asp102 of the structure TGT·**4** determined at 1.70 Å. The map clearly shows that the side chain of Asp102 occupies two different conformations. (Coordinates and structure factors for TGT·**4** taken from ref. [8].)* ►

although the sequence homology is rather low amounting to only 25 %.[8] This domain also folds into a TIM-barrel but the secondary structural elements are different to those in the *Z. mobilis* enzyme (Figure 4 b). In addition to the catalytic domain, the ArcTGT contains three C-terminal domains which altogether consist of about 300 amino acids. These domains adopt novel folds. The C3-domain possesses sequence homology to the "PUA" domain.[10] This domain is widely conserved among eukaryotic and archael RNA-modifying enzymes. Since the C-terminal domains contain conserved basic residues, it is assumed that they are involved in tRNA binding. The presence of these additional domains is probably a prerequisite for the difference in tRNA recognition between ArcTGT and QueTGT. Whereas prokaryotic TGT recognises the anticodon loop, archaebacterial TGT modifies the D-loop. Recently, the structure of *P horikoshii* in complex with tRNA has been determined to 3.3 Å resolution.[11] It could be confirmed that indeed the PUA domain interacts with the nucleic acid. But unexpectedly, an alternative tertiary structure of the tRNA (named the "λ form") has been detected. In this conformation, the canonical core is disrupted and the melted D-arm is protruded. In this conformation, those base pairs are disrupted that constitute, in the canonical tRNA conformation, the stem of the D-arm. While one strand of the former D-stem then base pairs with the otherwise unpaired variable loop, the second strand remains unpaired and, together with the D-loop, protrudes from the tRNA.

In contrast to the crystal structure of *Z. mobilis* TGT, in the ligand-free structure of *P. horikoshii* TGT, part of the active site (amino acids 97 – 106, which correspond to 104 – 113 in *Z. mobilis* TGT) is disordered. After substrate binding this part becomes ordered. Compared to *Z. mobilis* TGT, three out of six amino acids forming a direct interaction to the ligand are conserved. The amino-pyrimidinone moiety of the substrate forms the same type of interactions to Asp130, Gln169 and Gly196, which correspond in *Z. mobilis* TGT to Asp156, Gln203, Gly230 (Figure 5 a, b). The hydrophobic amino acids Met260 and Tyr106 of *Z. mobilis* TGT intercalating the substrate are replaced by Phe99

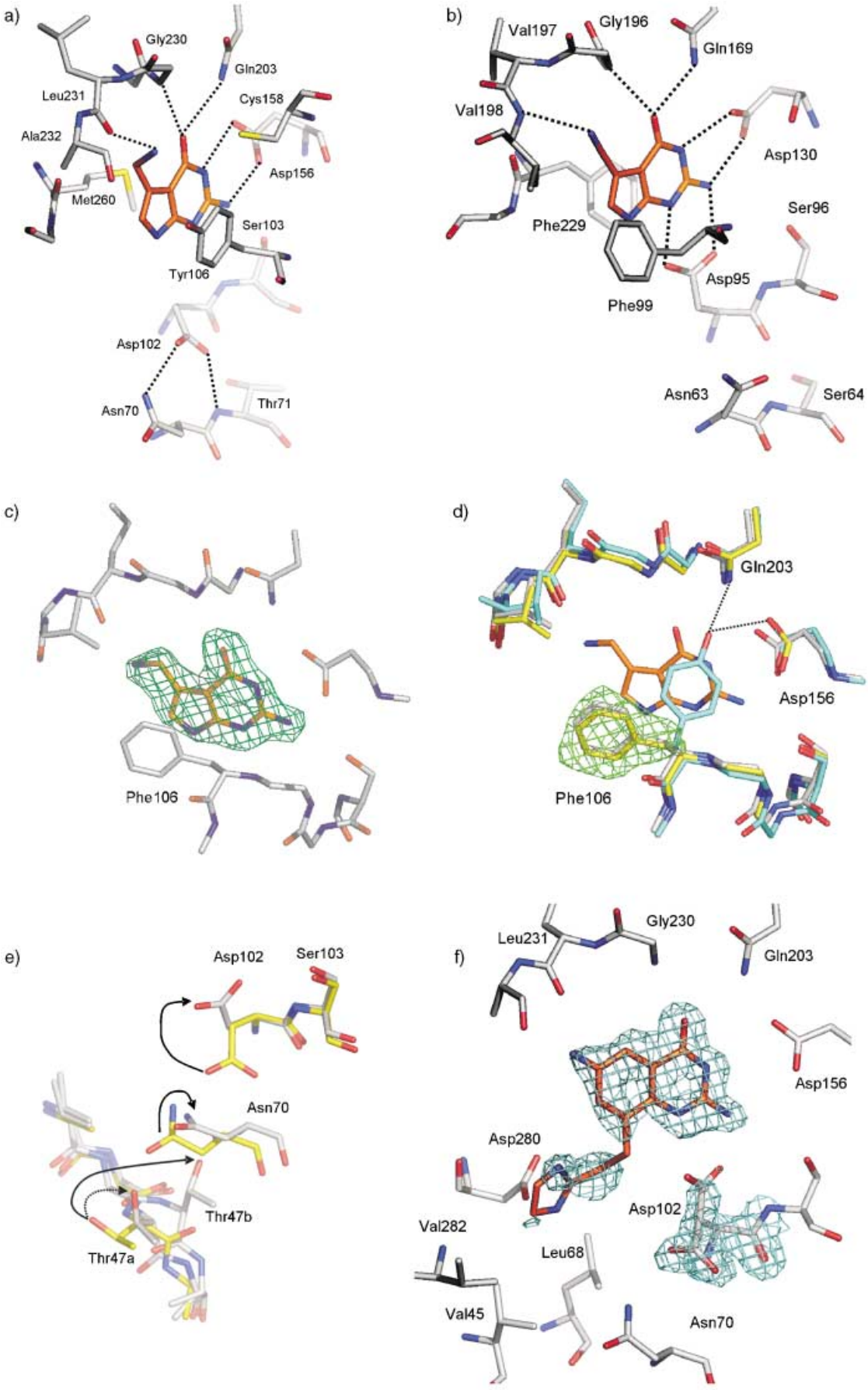

and Phe229. In addition, Leu231 (*Z. mobilis* TGT) is substituted by Val197. In this part of the binding pocket, an interesting difference is observed compared to *Z. mobilis* TGT. In the complex structure of *Z. mobilis* TGT·preQ$_1$ the carbonyl oxygen atom of Leu231 faces the binding pocket forming a hydrogen bond to the terminal amino group of the substrate. However, in the *P. horikoshii* TGT, the peptide bond from Val197 to Val198 is flipped. In consequence, the hydrogen atom of the adjacent amide group is now facing the binding pocket. This group donates a hydrogen bond to the cyano group of preQ$_0$ which shows hydrogen-bond acceptor properties. Furthermore, the side chain of the catalytic residue Asp95 is rotated towards the ligand to form two parallel hydrogen bonds.

No structure of a eukaryotic TGT has been determined to date. The sequence of the human TGT has been published recently.[12] It shares a sequence identity of 43% with the *Z. mobilis* TGT. Based on the crystal structure of *Z. mobilis* TGT Romier et al. have modelled the structure of the eukaryotic TGT of *C. elegans*.[8] According to this model, only a few amino acids need to be replaced in the active site. It is supposed that the replacement of Cys158 (*Z. mobilis* TGT) by Val has no major influence on substrate recognition (Figure 5a). Important, however, is the substitution of Val233 (*Z. mobilis* TGT) by glycine (see Figure 8b), which would open up the binding pocket in this region to accommodate the cyclopentendiol moiety of the natural substrate queuine.

The exact physiological role of incorporating queuosine and archaeosine into the tRNA remains unclear. It has been suggested that both bases play a role in stabilising a certain conformation of tRNA.[13, 14] Furthermore, the presence of queuosine in the wobble position may alter the efficiency and fidelity of tRNAs during translation.[15–17] In eukaryotes, queuosine is probably involved in differentiation, proliferation, cellular signalling and the oxidative stress response.[18] In addition, the tRNA of tumours is often undermodified with respect to queuosine.[19] On the other hand, leukemic cells exhibit an increased queuosine level in tRNA.[20] *E. coli* cells lacking the *tgt* gene show no significant change in growing behaviour.[21] However, *S. flexneri* cells lacking this gene show a dramatically reduced virulence phenotype.[22] This change is due to an insufficient translation of *virF* mRNA that encodes a regulator protein involved in the expression of several important virulence proteins.[23] This situation prompted us to use the TGT as a target for the design of new antibiotics against Shigellosis.[24–27]

Herein we discuss flexible adaptations of the substrate binding pocket of *Z. mobilis* TGT that have an impact on substrate selectivity, on the assumed reaction mechanism and which provide new concepts for structure-based drug design.

Results and Discussion

Flexible Adaptations in the Protein

Closed and Opened Binding Pocket

For the determination of K_i values of competitive inhibitors with the *Z. mobilis* enzyme, a preincubation step of about 20 min is required.[27] This step is not necessary in the case of the *E. coli* enzyme, which exhibits a sequence identity of about 52% to the *Z. mobilis* enzyme and exposes a phenylalanine towards the active site.[28] Apart form this replacement, the binding pockets of both enzymes are identical. The crystal structure of the ligand-free *Z. mobilis* enzyme shows that the binding pocket is closed by Tyr106 (Phe106 in Figure 5d) which forms hydrogen bonds to Asp156 and Gln203 (Figure 5d).[7] Note that most TGTs possess a Phe instead of a Tyr residue at this position. A search in the SWISS-Prot database (posted date May 24, 2003)[29] revealed that out of 53 sequences having a sequence identity of more than 34% with *Z. mobilis* TGT, only the one originating from the thermophilic bacterium *Aquifex aeolicus* also contains this tyrosine residue. Are the hydrogen bonds formed with the additional hydroxy group of Tyr106 responsible for the deviating kinetic behaviour? To address this question we constructed a Y106F mutant of *Z. mobilis* using site-directed mutagenesis. The mutated protein crystallised similarly to the wild type. The crystal structure of TGT(Y106F) in complex with the natural substrate preQ$_1$ was determined at 1.90 Å resolution. The $|F_o|-|F_c|$ electron density with the ligand omitted from the calculation (contoured at 2.5 σ) clearly defines the substrate (Figure 5c), which adopts the same binding mode as in the structure of the wild-type enzyme.[7]

As described above, the side chain of Tyr106 blocks the binding pocket by forming hydrogen bonds to neighbouring amino acids. In the uncomplexed structure of *P. horikoshii* this part of the binding pocket is disordered. Thus, it raises the question, which conformation the corresponding amino acids would adopt in the uncomplexed structure of the mutated *Z. mobilis* TGT? This structure was determined at 1.95 Å. As the starting geometry for the refinement, we used the coordinates of the ligand-free structure of the wild-type enzyme, but replaced Tyr106 by alanine. The positive $|F_o|-|F_c|$ electron-density map (contoured at 2.5 σ) clearly shows that Phe106 adopts the open conformation supposedly favourable for substrate binding (Figure 5d).

To check whether the observed preorganisation of Phe106 influences the required preincubation time, we determined the kinetic parameters of the mutated enzyme. With both substrates, tRNA as well as [^{3}H]-guanine, K_m, k_{cat} and k_{cat}/K_m remained unchanged within the error limits of the measurements compared to the wild-type enzyme (Table 2, Figure 7).[30, 31] Accordingly, the mutated enzyme shows kinetics similar to those of the wild type.

With ligand **1** (Figure 6), an inhibitor of *Z. mobilis* TGT,[27] the influence of the preincubation time on the initial velocity of the enzyme reaction was examined. For this purpose, the mutated enzyme was preincubated at a given ligand concentration and the reduction in the velocity was plotted against time. After a preincubation time of twelve minutes the initial velocity dropped to about 60% of the starting value (Figure 7b). Preincubation for an additional eight minutes did not reduce the velocity. The same behaviour was found for the wild-type enzyme[27] showing that the preorganisation of Phe106 does not correlate with the required preincubation. Therefore, the rupture of the hydrogen-bond network at the door-keeping Tyr106 can be ruled out as a direct explanation of the preincubation

Table 2. *Kinetic characterisation of the TGT(Y106F) mutant with tRNA and [^{3}H]-guanine as substrate.*[a]

tRNA Parameter	TGT (w.t.)	TGT(Y106F)
K_m [μM]	1.0 ± 0.4	0.36 ± 0.1
v_{max} [μM min^{-1}]	$61.5 \times 10^{-3} \pm 4.3 \times 10^{-3}$	$44.7 \times 10^{-3} \pm 6.7 \times 10^{-3}$
k_{cat} [s^{-1}]	$1.4 \times 10^{-2} \pm 0.1 \times 10^{-2}$	$0.5 \times 10^{-2} \pm 0.1 \times 10^{-2}$
k_{cat}/K_m [μM^{-1} s^{-1}]	$13.9 \times 10^{-3} \pm 1.0 \times 10^{-3}$	$13.3 \times 10^{-3} \pm 1.4 \times 10^{-3}$
[^{3}H]-guanine Parameter	TGT (w. t.)	TGT(Y106F)
K_m [μM]	0.38 ± 0.1	1.3 ± 0.1
v_{max} [μM min^{-1}]	$48.8 \times 10^{-3} \pm 3.3 \times 10^{-3}$	$38.9 \times 10^{-3} \pm 4.0 \times 10^{-3}$
k_{cat} [s^{-1}]	$1.1 \times 10^{-2} \pm 0.1 \times 10^{-2}$	$0.4 \times 10^{-2} \pm 0.04 \times 10^{-2}$
k_{cat}/K_m [μM^{-1} s^{-1}]	$28.9 \times 10^{-3} \pm 8.3 \times 10^{-3}$	$3.4 \times 10^{-3} \pm 0.2 \times 10^{-3}$

[a] For comparison, the values of the wild-type enzyme are also given.[30] Within the error limits, the values are identical for both enzymes

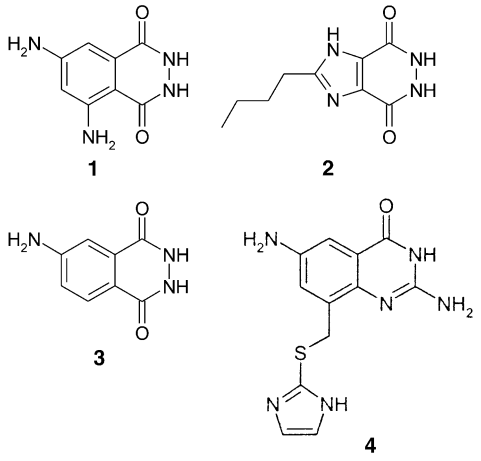

Figure 6. *Inhibitors of* Z. mobilis *TGT.*

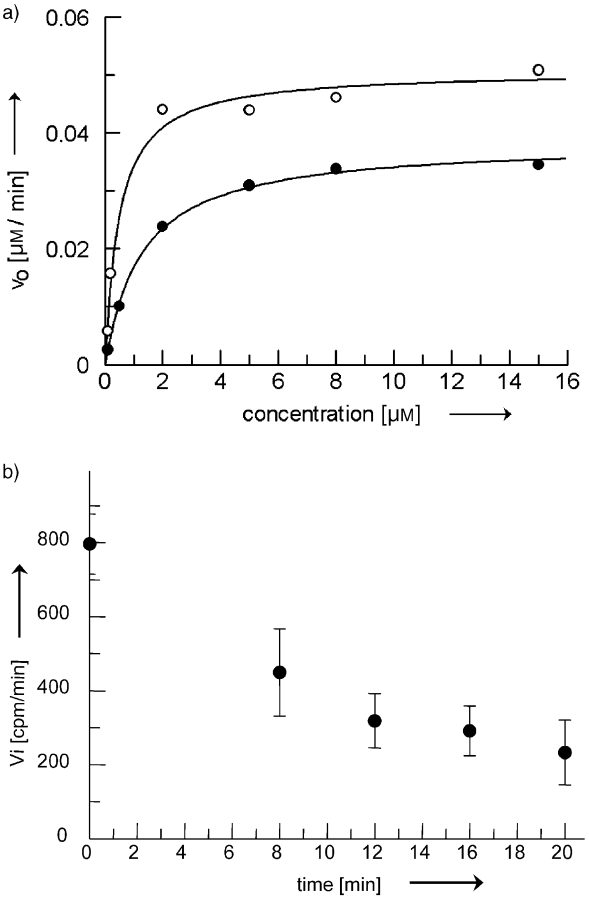

Figure 7. *a) Michaelis – Menten plot of TGT(Y106F). ○ values for varying tRNA concentrations and a fixed guanine concentration; ● values for varying guanine concentrations and a fixed tRNA concentration. The solid lines indicate a regression calculated through these values V_0 = initial velocity. b) Influence of the mutation Y106F on the preincubation time of ligands for determining K_i values. Compound* ***1*** *was added in a final concentration of 50 μM to the mixture of mutated enzyme and substrate. The initial velocity V_i was determined after 0, 8, 12, 16 and 20 min. The error bars indicate the estimated standard deviation of two measurements. CPM = counts per minute.*

phenomena. Clearly, other structurally less evident factors are responsible for this behaviour.

Substrate Selectivity

As mentioned in the Introduction, the TGTs of the three kingdoms differ in substrate specificity (Table 1).[4–6] The most pronounced substrate selectivity is shown by archaebacterial TGTs. They exclusively accept their natural substrate $preQ_0$ in addition to guanine. Note that in the crystal structure of ArcTGT·$preQ_0$ the cyano group of this ligand is hydrogen bonded to the amide nitrogen atom of Val198 (Ala232 in *Z. mobilis* TGT Figure 5a, b) whereas in the crystal structure of the prokaryotic TGT in complex with $preQ_1$, the terminal nitrogen atom of the ligand's amino group donates a hydrogen atom to the carbonyl group of Leu231 (Val197 in *P. horikoshii* TGT; Figure 5a, b). To achieve this binding mode, the peptide bond between Leu231 and Ala232 in *Z. mobilis* TGT is flipped compared to the corresponding bond in *P. horikoshii* TGT (Val197 to Val198). Accordingly, in the crystal structure of *Z. mobilis* TGT an acceptor group is presented towards the binding pocket, whereas in *P. horikoshii* TGT a donor group is presented. These swapped functionalities are responsible for the deviating recognition properties with respect to natural substrates $preQ_0$ and $preQ_1$. Interestingly, this flip of the backbone can be provoked or induced in prokaryotic TGT by ligand binding or a pH shift. Recently, we have reported on a ligand (**2**, Figure 6) which adopts an unexpected new binding mode,[24] where the peptide bond between Leu231 and Ala232 has been flipped compared to the uncomplexed structure (Figure 5d and Figure 8b). The conformation observed in this flipped structure matches well with the one found in ArcTGT (Figure 5b). Furthermore, an interstitial water molecule (W1) mediates the contact between the ligand and this region of the binding pocket (Figure 8b). A very similar binding mode was detected for guanine in the ArcTGT.[9] In this case, the contact between ligand and protein is also mediated by an interstitial water molecule.

To increase the solubility of basic ligands in the soaking buffer, we established crystallisation conditions at pH 5.5. A structure of

the uncomplexed enzyme, crystallised under these conditions, could be determined with a resolution of 1.90 Å. At this pH value, several differences to the ligand-free structure crystallised at pH 8.5 are apparent. The general fold remains unchanged, but in two regions exhibiting enhanced high temperature factors at pH 8.5 (>45 Å^2 or >70 Å^2, average for remaining residues 20.7 Å^2)[7] the structure is modified. Both regions experience a relatively high content of amino acids that are probably charged (Lys125, His127, Asp129, Arg132 in one region and His133 or Arg286 and Arg289 in the other). In the region represented by the β-strands 7–9 (Figure 4a), the degree of disorder increases and strand 9 becomes completely disordered. In contrast, helix 12 is much more ordered at pH 5.5 than at pH 8.5 (Figure 8d). The average temperature factor for these amino acids drops to 29.3 Å^2. Furthermore, in the substrate binding pocket, the backbone flip of the peptide bond Leu231 to Ala232 is induced (Figure 8e). The adopted conformation exactly matches that found in TGT·**2**, with the addition of a new water molecule (W6). This water molecule is hydrogen bonded to the flipped carbonyl group of Leu231 (Figure 8e).

Superposition of the ligand-free crystal structure (pH 5.5) of *Z. mobilis* TGT containing the flipped backbone conformation with the corresponding region of *P. horikoshii* TGT reveals that one carboxylate oxygen atom of Glu235 (*Z. mobilis* TGT) fits onto the nitrogen atom of the peptide bond Pro199 to Leu200 (*P. horikoshii* TGT; Figure 8e). This nitrogen atom forms a hydrogen bond to the carbonyl group of Val197. In the structure of the *Z. mobilis* enzyme, the distance between the carboxylate oxygen atom of Glu235 superimposed with the amide nitrogen atom of Leu200 in *P. horikoshii* TGT and the carbonyl group of Leu231 (Val197 in *P. horikoshii* TGT) is only 2.4 Å. If Glu235 is deprotonated, the interaction between these atoms should create an unfavourable repulsive acceptor–acceptor interaction, which suggests that Glu235 might act as a general acid/base. Depending on the given pH value or induced by a bound ligand, this carboxylate group switches between a protonated or deprotonated state, which stabilise the two alternative backbone conformations.

If *Z. mobilis* TGT is cocrystallised with preQ$_0$ at pH 5.5, again the flipped conformation of the Leu231–Ala232 peptide bond which exposes the NH donor facility is present (Figure 8a). In this structure, the water molecule W1 found in QueTGT·**2** is replaced by the cyano group of preQ$_0$ which forms a hydrogen bond to the NH group of Ala232 (Figure 8b). Compared to the TGT·**2** complex and the ligand-free structure at pH 5.5 a remarkable change in this part of the protein becomes apparent. Part of a loop starting from Val233 and running to Glu235 is shifted downwards and the peptide bond between Glu235 and Gly236 is also flipped (Figure 8c). Furthermore, the carbonyl group of Leu231 no longer forms a hydrogen bond to Glu235 but only interacts with water molecule W6, whereas the side-chain carboxylate group of Glu235 stacks with its hydrophobic π face on top of the adjacent peptide bond. Thus instead of directly interacting through a hydrogen bond, the two functional groups interact through their hydrophobic moieties which are exposed perpendicular to the functional-group planes.

Figure 8. *a) $2|F_o|-|F_c|$ electron-density map of TGT·preQ$_0$ (contoured at 1.0 σ, cyan) and $|F_o|-|F_c|$ map (contoured at 2.5 σ, green). The cyano group of preQ$_0$ forms a hydrogen bond to Ala232. The carbonyl group of Leu231 is hydrogen bonded to W6. b) Superposition of* Z. mobilis *TGT·preQ$_0$ (grey, ligand orange) with TGT·**2** (yellow, ligand cyan). Both structures display a flipped backbone conformation at the peptide bond Leu231 to Ala232. Part of a loop composed by the amino acids Val233 to Glu235 is shifted downward in TGT·preQ$_0$ compared to TGT·**2**. (Coordinates for TGT·**2** taken from ref. [24].) c) Superposition of* Z. mobilis *TGT·preQ$_0$ (grey) with TGT·**2** (yellow). In TGT·**2** Glu235 is hydrogen-bonded to Leu231 whereas in TGT·preQ$_0$ the terminal carboxylate group of Glu235 stacks with its hydrophobic π face on top of the peptide bond Leu231 to Ala232 and an additional water molecule (W6) is found in hydrogen-bonding distance to the carbonyl group of Leu231. (Coordinates for TGT·**2** taken from ref. [24].) d) Part of the X-ray structure of* Z. mobilis *TGT that is better ordered at pH 5.5 together with the $2|F_o|-|F_c|$ electron-density map (contoured at 1.0 σ). e) Superposition of the crystal structure of uncomplexed* Z. mobilis *TGT, crystallised at pH 5.5 (grey) with that of* P. horikoshii *TGT (green). In* P. horikoshii *TGT a hydrogen bond is formed between Val197 and Leu200 whereas in* Z. mobilis *TGT a hydrogen bond is formed from Leu231 to Glu235 – assuming that Glu235 is protonated. (Coordinates for* P. horikoshii *TGT taken from ref. [9].) f) $2|F_o|-|F_c|$ electron-density map (contoured at 1.0 σ, cyan) and $|F_o|-|F_c|$ map (contoured at 2.5 σ, green) of* Z. mobilis *TGT·preQ$_1$, cocrystallised at pH 5.5.*

Thus, Glu235 seems to play an important role for substrate selectivity. This hypothesis is supported by a sequence analysis of TGTs across different organisms. Among prokaryotic and eukaryotic TGTs, which accept both substrates, preQ$_1$ and preQ$_0$, this glutamate 235 is highly conserved.[8] In contrast, the backbone of *P. horikoshii* TGT is conformationally restricted in this region by Pro199 (Figure 8e). Therefore, the decreased flexibility of the Val197–Val198 peptide bond as well as the absence of a general acid/base in this region prevents the peptide-bond switching and could explain the enhanced substrate selectivity of archaebacterial TGT compared to prokaryotic and eukaryotic TGTs. It is remarkable that for *Z. mobilis* TGT, substrate selectivity is determined not by the amino acids directly exposed towards the active site but more by those residing in the peripheral sphere.

It remains unclear in this context, why in the structure QueTGT·preQ$_0$, cocrystallised at pH 5.5, the amino acids Val233 to Glu235 (Figure 8b) are shifted compared to the complex QueTGT·**2**, obtained by soaking at pH 8.5. Clearly, a direct contact with a hydrogen-bonding distance is avoided. Whether this is due to the difference in pH value resulting in the different protonation states of Glu235, the cocrystallisation procedure or to the different nature of the ligands creating different local dielectric conditions is a matter of further investigations.

Catalytical Aspartate

The reaction catalysed by TGT follows an associative mechanism that proceeds via a covalent intermediate (Figure 1).[2, 3] In the case of *Z. mobilis* TGT the covalent bond is presumably formed to Asp102 which nucleophilicly attacks the ribose carbon C4 of nucleoside 34 of the tRNA. In the structure of QueTGT·preQ$_1$ (pH 7.3) the side chain of this aspartate residue points away from the required reaction site. Instead, it is hydrogen-bonded to Asn70 and Thr71 (Figure 5a). Consequently, Romier et al.

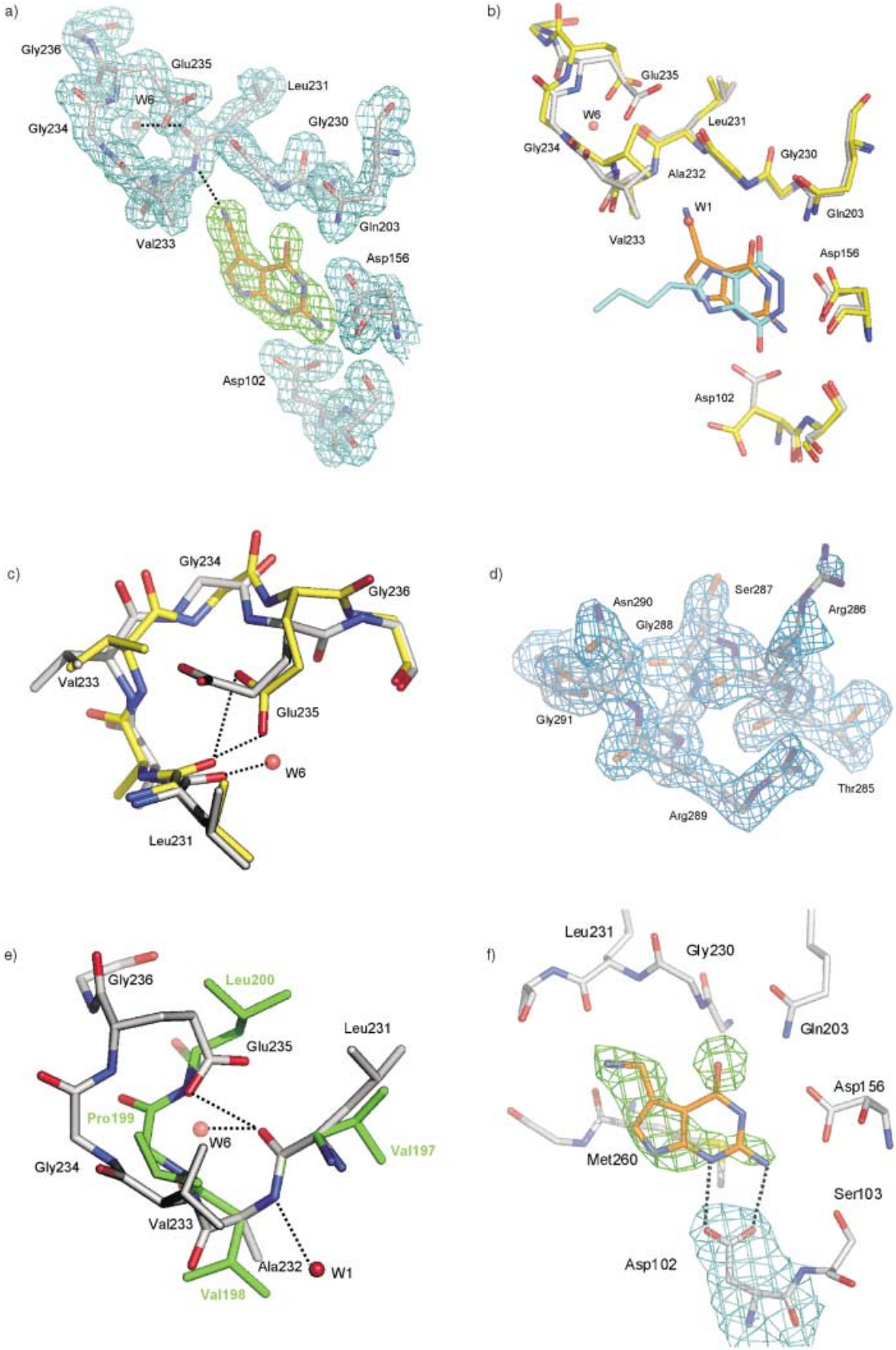

assumed that the binding of tRNA is a prerequisite for breaking these hydrogen bonds and that the breaking of these bonds enables Asp102 to accomplish its catalytic function.[7] In a subsequent paper Romier et al. described mutated variants of *Z. mobilis* TGT.[3] In the uncomplexed structures of TGT(D156A) and TGT(D156Y) a rotation of Asp102 of about 180° into the binding site was found. This change suggested that the hydrogen-bond network could probably be broken without tRNA binding. In the case of *P. horikoshii* TGT, the side chain of the corresponding Asp95 residue is rotated into the binding pocket both in the ligand-free structure and in the presence of the ligand.[9] It forms two parallel hydrogen bonds to an accommodated ligand, this conformation requires that either the ligand or the aspartate is protonated (Figure 5b). Since Asn70 of *Z. mobilis* TGT is also present in *P. horikoshii* TGT (Asn63), the conformation of Asp102 found in the structure of TGT·preQ$_1$ could in principle be adopted by Asp95 of *P. horikoshii* TGT. Both crystals, those of ArcTGT and of QueTGT, have been soaked with their substrates at pH 7.5.[7, 9] To check whether a lower pH value during soaking the QueTGT crystals would result in a rotation of Asp102 as seen in ArcTGT, we soaked a crystal with preQ$_1$ at pH 5.5. However, at this pH value, soaking of preQ$_1$ was no longer successful as the crystals dissolved. Cocrystallisation of preQ$_1$ with QueTGT at pH 5.5 resulted in crystals with the new space group C222$_1$ (Table 3). The crystals did not diffract quite as well but a dataset of 2.40 Å resolution could be collected. The packing in the new space group did not alter significantly the crystal contacts or the shape of the enzyme. The overall root-mean-square deviation (rmsd) of all the C_α atoms of TGT·preQ$_0$ and TGT·preQ$_1$ amounts to only 0.32 Å. In this structure, the side chain of Asp102 is rotated towards the ligand as in ArcTGT (Figure 8f). This rotated conformation was also found in QueTGT·preQ$_0$, which was cocrystallised at pH 5.5 (Figure 8a). These results indicate that the rearrangement of Asp102 is indeed induced by the bound base even in absence of tRNA.

The basic pK_a value of N1 in preQ$_0$ (Figure 3) is < 1 whereas the pK_a of N1 in preQ$_1$ is about 1.8.[32] For the side chain of free aspartate, a pK_a value of 3.9 is measured in water.[33] To form a hydrogen bond between Asp102 in QueTGT or Asp95 in ArcTGT and the bound substrate, either the side chain or the ligand must be protonated. Accordingly, a pK_a shift is induced by the bound ligand.

Because of the rearrangement of Asp102, several additional changes occur in the structure as a cascade of subsequent "domino effects". As Asn70 is no longer hydrogen bonded to Asp102, part of its side chain becomes disordered. Furthermore, compared to TGT·**2**, Asn70 is slightly shifted towards Asp102 (Figure 5e). In consequence additional space between Asn70 and Thr47 is created resulting in the population of an alternative conformer of Thr47.

Structure-Based De Novo Design

As TGT is a prerequisite of the efficient pathogenicity of *Shigellae*, the causative agent of dysentery,[22, 23] the structure of *Z. mobilis* TGT has been used in structure-based drug design.[24–27] In a first design cycle, the crystal structure of the TGT·preQ$_1$ complex served as a basis for the de novo design of ligands using the program LUDI.[27, 34] Through this approach, 4-aminophthalhydrazide (**3**; Figure 6) was discovered as a first lead structure in the low micromolar range. The crystal structures of TGT together with this inhibitor, as well as with several extended derivatives were determined. All of them showed no significant side-chain

Table 3. *Data collection and refinement statistics.*

Crystal data	TGT(Y106F)	TGT(Y106F)·preQ1	TGT·preQ$_0$	TGT (pH 5.5)	TGT·preQ$_1$
Space group	C2	C2	C2[a]	C2[a]	C222$_1$[a]
Cell constants					
a [Å]	90.39	90.25	90.62	90.38	64.47
b [Å]	64.72	65.02	65.54	65.37	91.87
c [Å]	71.88	71.40	70.33	70.57	165.83
β [°]	97.02	96.65	96.46	96.30	90.00
Resolution [Å]	40.00 – 1.95	40.00 – 1.90	20.00 – 1.70	40.00 – 1.90	25.00 – 2.40
Total no. of reflections	109129	98882	163734	116335	94879
No. of unique reflections	29077	31900	43081	32280	19371
Completeness of all data ([%], outer shell)	96.4 (94.0)	98.2 (96.3)	95.6 (92.2)	99.9 (99.8)	97.9 (99.5)
R_{symm} for all data ([%], outer shell)[b]	7.0 (29.4)	6.4 (27.4)	10.4 (56.2)	7.1 (24.4)	9.6 (42.0)
R_{free} [%][c]	19.8	21.1	20.0	20.9	25.2
R factor [%][c]	18.4	18.0	17.6	17.2	20.6
No. of protein atoms (non-hydrogen atoms)	2895	2907	2930	2830	2828
No. of water molecules	342	365	377	358	116
rmsd angle [°]	1.2	1.2	1.4	1.2	1.3
rmsd bond [Å]	0.005	0.005	0.008	0.005	0.007
average *B* factors, protein atoms [Å^2]	20.9	20.8	20.0	20.8	38.8
average *B* factors, water atoms [Å^2]	30.7	30.9	31.0	30.5	35.3
average *B* factors, ligand atoms [Å^2]	-	22.1	19.1	-	38.8

[a] ϕ and ψ angles remain in the same area a found in the structure of Romier et al. (1PUD).[7] [b] $R_{symm} = \Sigma | I - < I > | \Sigma I$, where I is the observed intensity and $< I >$ is the average intensity for multiple measurements. [c] The R_{free} [46]was calculated from a random selection of reflections constituting ≈ 10 % of the data; the *R* factor was calculated with the remaining intensities. [d] rmsd = root-mean-square deviation.

or backbone movements when compared to TGT·preQ$_1$. A topological search for ligands sharing the dihydropyridazinedione scaffold of **3** retrieved several ligands that actually showed K_i values in the micromolar range.[24] Out of these compounds, the crystal structure of TGT complexed with **2** could be determined (Figure 8b). This structure was the first to show the flip of the peptide bond between Leu231 and Ala232, such that the NH group of the amide bond is exposed to the binding pocket. In addition, an interstitial water molecule mediated a contact between this peptide bond and the ligand. As described above, this binding mode is very similar to that detected in ArcTGT·guanine, Arc·preQ$_0$[9] and QueTGT·preQ$_0$ (Figure 5b, Figure 8a). The finding of this binding mode prompted us to develop a composite pharmacophore model. Virtual screening based on this multiple-protein-based pharmacophore resulted in hits for distinct compound classes. In the kinetic assay they exhibited affinities in the micromolar to the submicromolar range.

In another design cycle, inhibitors with a quinazolinone scaffold were designed as an alternative lead skeleton (e.g. **4**, Figure 6).[26] This scaffold was assumed to mimic the interactions of preQ$_1$ in the binding pocket. The predicted binding mode could be confirmed by crystal-structure analysis (Figure 5f) with a crystal that was soaked at pH 8.5. Surprisingly, after refinement, in addition to the expected interactions, two conformations of Asp102 become visible in the $2|F_o|-|F_c|$ electron-density map (contoured at 1.0 σ): In one conformation, Asp102 is still hydrogen bonded to Asn70 as found in QueTGT·preQ$_1$ at pH 7.3, in the other conformation, Asp102 forms hydrogen bonds with the ligand as in the complexes QueTGT·preQ$_1$ and QueTGT·preQ$_0$ cocrystallised at lower pH value (Figure 5f, Figure 8a). Compared to the natural substrates, this compound class possesses an elevated pK_a value (about 4.5), which may account for the rearrangement of Asp102 observed even at higher pH. The refined data do not allow us to determine whether both conformations occur in the presence of the bound ligand. Since the active site is only partially occupied, it is possible that only protein molecules with the bound ligand exhibit the rearranged conformation, whereas all the uncomplexed molecules orient Asp102 away from the ligand binding site. Attempts to design ligands with an alternative scaffold that places a positively charged group between Asp102 in its rotated ligand-exposed conformation and Asp156 are in progress.

As Asn70 is no longer fixed to Asp102 in its rearranged orientation, a small hydrophobic pocket formed by Val45, Leu68 and Val282 (Figure 5f) increases in size. This pocket has already been addressed successfully by aromatic substituents.[25, 26] Consequently we plan to fill the expanded pocket by larger and shape-complementary substituents.

Conclusion

The enzymes TGT catalyse the post-transcriptional modification of tRNA by the introduction of modified bases. The orthologous proteins of *Z. mobilis* and *E. coli* differ in only one residue in the active site: Tyr106 is replaced by phenylalanine. Nevertheless, they show a different kinetic behaviour in response to competitive inhibitors, for example, the *Z. mobilis* enzyme requires a preincubation step for inhibition. We could show by a mutational study of TGT(Y106F), that although in contrast to Phe106, the residue Tyr106 is hydrogen bonded in the ligand-free structure, this is not the reason for the kinetic difference. Clearly, other structurally less evident factors are responsible for this behaviour.

Further, the different enzymes originating from the three kingdoms of life differ in their substrate selectivity. Structural evidence could be collected to describe and understand the deviating potential of the active sites of the enzymes to adopt and subsequently accommodate the different substrates. Remarkably, a peptide-bond flip, triggered by pH conditions and/or induced by ligand binding, modulates the recognition properties of the substrate binding site which switch between hydrogen-bond donor and acceptor functionality. Furthermore, interstitial water molecules are used to complement the versatile adaptations of the pocket. The peptide switch is stabilised by an adjacent glutamate residue present in the next coordination sphere around the substrate binding pocket that operates as a general acid/base by changing its protonation state depending on the bound ligand. The plasticity of this part of the binding pocket together with the properties of the interstitial water molecule have been exploited in the design of novel inhibitors. An active-site aspartate residue, assumed to operate as a nucleophile through covalent bonding during the base-exchange reaction, has different conformations depending on the chemical nature of the bound ligand. Since the rearrangement of this residue is required for catalysis and has consequences for the shape of an adjacent hydrophobic sub-site, the observed structural adaptations will be used in a subsequent ligand-design concept. Interestingly enough, the induced-fit adaptations experienced by TGT and discovered through multiple crystal-structure analysis of ligand–protein complexes all affect the functional properties of the enzyme. Once detected and mechanistically understood this plasticity can be exploited for the design of structurally distinct inhibitors.

Experimental Section

Z. mobilis TGT, both wild-type and Y106F mutant, were prepared as described elsewhere.[31, 35] *E. coli* tRNA^{Tyr} was prepared as described by Curnow et al.[36]

Construction of the TGT mutant Y106F: Site-directed mutagenesis was performed using the QuickChange kit (Stratagene).[37] The oligonucleotides listed in Table 4 were used to construct Y106F with pET9d-ZM[31] serving as template. Successful mutagenesis was verified by sequence analysis of the complete mutated *tgt* gene.

Determination of kinetic parameters and preincubation time: The kinetic parameters of the mutated TGT were determined as described elsewhere[30] which is a modification of the assay described in ref. [31]. For the varied substrate, concentrations of up to 15 μM were used, whereas the fixed substrate was added in a final concentration of 20 μM. Michaelis–Menten parameters were determined in triplicate and the values given in Table 2 are the average of these measurements. The initial velocities of the enzyme reaction inhibited with ligand **1** (50 μM) were determined after 0 to 20 min preincubation time as described by Grädler et al.[27]

Table 4. *Oligonucleotides used in mutagenesis.*

Oligo	Sequence (5′ to 3′).[a]
Y106F-s	5′-G ACG GAT AGC GGC GGG *TTC* CAG GTG ATG AGC CTA TC-3′
Y106F-a	5′-GA TAG GCT CAT CAC CTG *GAA* CCC GCC GCT ATC CGT C-3′

[a] The mutated codon is italicised.

Crystallisation, soaking and cocrystallisation: Wild-type TGT and TGT(Y106F) where crystallised at pH 8.5 as described elsewhere.[35] For crystallisation at pH 5.5, first crystals for macro seeding where obtained out of a mixture of TGT (2 μL, 14 mg mL^{-1}) dissolved in the buffer described in ref. [35] along with 2 μL of a buffer composed of morpholino ethylsulfonate (MES; 100 mM), pH 6.0, dithiothreitol (DTT; 1 mM), poly(ethylene glycol) (PEG 8.000 10% (w/v)) and DMSO (10% (v/v)) by the hanging-drop method with the latter solution also serving as the reservoir solution. These drops were seeded with small crystals grown at pH 8.5. Seed crystals obtained under these conditions within two days were then transferred into a mixture of 2 μL, 14 mg mL^{-1} TGT with 2 μL of MES (100 mM), pH 5.5, DTT (1 mM), PEG 8.000 (8% (w/v)) and DMSO (10% (v/v)) and allowed to grown further using the hanging-drop method. Crystals with a size of approximately $0.7 \times 0.7 \times 0.2$ mm grew within five to seven days.

$preQ_1$ and $preQ_0$ for soaking and cocrystallisation experiments were synthesised as described in ref. [38] and ref. [39], respectively.

Soaking of $preQ_1$ in crystals of TGT(Y106F) was performed as described elsewhere.[27] As soaking of $preQ_0$ was unsuccessful at pH 8.5 and pH 5.5 and for $preQ_1$ at pH 5.5, these compounds were cocrystallised at pH 5.5. For this purpose, the ligands were dissolved in the buffer at pH 5.5 described above in (50 mM $preQ_1$ and saturation concentration of $preQ_0$ (< 50 mM). The crystallisation was performed by macro seeding as described above.

Structure determination: X-ray data (Table 3) were collected at $-173\,^{\circ}C$ as described elsewhere.[27] Diffraction data were processed using the programs DENZO and SCALEPACK.[40] The structures were refined through several cycles of least-squares refinement along with an energy minimisation using CNS.[41] Manual adjustments to the electron density have been performed using O.[42] Molecular replacement for TGT·$preQ_1$ was calculated using AMoRe.[43]

Potentiometric measurement of ionization constants (pKa): The measurements were performed as described elsewhere[27] but owing to the low solubility of the compounds in water, 10% DMSO was added for the standardization of the electrode and the titration of the ligand.

Figures: Figure 4 was produced using TopDraw,[44], Figure 5 and Figure 8 were produced using PyMOL.[45]

Protein Data Bank accession codes: The coordinates for the structures TGT(Y106F), TGT(Y106F)·$preQ_1$, TGT·$preQ_0$, TGT (crystallised at pH 5.5) and TGT·$preQ_1$ have been deposited in the RCSB Protein Data Bank, with the accession codes 1OZM, 1OZQ, 1P0B, 1P0D and 1P0E, respectively.

Acknowledgements

This work was supported by the Deutsche Forschungsgemeinschaft (Grant KL-1204/1). We thank C. Sohn for his assistance in the X-ray measurements, G. A. Garcia for samples of $preQ_1$ and $preQ_0$ and Tanja Sgraja for help in site-directed mutagenesis.

Keywords: drug design · induced-fit adaptions · multiple substrate recognition · substrate selectivity · RNA

References

[1] R. K. Slany, H. Kersten, *Biochimie* **1994**, *76*, 1178 – 1182.
[2] J. D. Kittendorf, L. M. Barcomb, S. T. Nonekowski, G. A. Garcia, *Biochemistry* **2001**, *40*, 14 123 – 14 133.
[3] C. Romier, K. Reuter, D. Suck, R. Ficner, *Biochemistry* **1996**, *35*, 15 734 – 15 739.
[4] N. Shindo-Okada, N. Okada, T. Ohgi, T. Goto, S. Nishimura, *Biochemistry* **1980**, *19*, 395 – 400.
[5] M. Watanabe, M. Matsuo, S. Tanaka, H. Akimoto, S. Asahi, S. Nishimura, J. R. Katze, T. Hashizume, P. F. Crain, J. A. McCloskey, N. Okada, *J. Biol. Chem.* **1997**, *272*, 20 146 – 20 151.
[6] N. Okada, S. Nishimura, *J. Biol. Chem.* **1979**, *254*, 3061 – 3066.
[7] C. Romier, K. Reuter, D. Suck, R. Ficner, *EMBO. J.* **1996**, *15*, 2850 – 2857.
[8] C. Romier, J. E. Meyer, D. Suck, *FEBS Lett.* **1997**, *416*, 93 – 98.
[9] R. Ishitani, O. Nureki, S. Fukai, T. Kijimoto, N. Nameki, M. Watanabe, H. Kondo, M. Sekine, N. Okada, S. Nishimura, S. Yokoyama, *J. Mol. Biol.* **2002**, *318*, 665 – 677.
[10] L. Aravind, E. V. Koonin, *J. Mol. Evol.* **1999**, *48*, 291 – 302.
[11] R. Ishitani, O. Nureki, N. Nameki, N. Okada, S. Nishimura, S. Yokoyama, *Cell* **2003**, *113*, 383 – 394.
[12] K. L. Deshpande, J. R. Katze, *Gene* **2001**, *265*, 205 – 212.
[13] J. M. Gregson, P. F. Crain, C. G. Edmonds, R. Gupta, T. Hashizume, D. W. Phillipson, J. A. McCloskey, *J. Biol. Chem.* **1993**, *268*, 10 076 – 10 086.
[14] R. C. Morris, K. G. Brown, M. S. Elliott, *J. Biomol. Struct. Dyn.* **1999**, *16*, 757 – 774.
[15] L. Curran in *Modification and Editing of RNA* (Eds.: H. Grosjean and B. Benne), American Society for Microbiology Press, Washington, DC, **1998**, pp. 493 – 516.
[16] G. R. Björk in *tRNA: Structure, Biosynthesis, and Function* (Eds.: D. Söll and U. L. Rajbhandary), American Society for Microbiology Press, Washington, DC, **1995**, pp. 165 – 205.
[17] G. Björk in *Escherichia coli and Salmonella: Cellular and Molecular Biology* (Eds.: F. C. Neidhardt, R. I. Curtiss, J. L. Ingraham, E. C. C. Lin, K. B. Low, B. Magasanik, W. S. Reznikoff, M. Riley, M. Schaechter and H. E. Umbarger), American Society for Microbiology Press, Washington, DC, **1996**, pp. 861 – 886.
[18] G. R. Björk, T. Rasmuson in *Modification and Editing of RNA* (Eds.: H. Grosjean and R. Benne), ASM Press, Washington DC, **1998**, pp. 493 – 615.
[19] U. Gündüz, M. S. Elliott, P. H. Seubert, J. A. Houghton, P. J. Houghton, R. W. Trewyn, J. R. Katze, *Biochim. Biophys. Acta* **1992**, *1139*, 229 – 238.
[20] S. Ishiwata, J. Katayama, H. Shindo, Y. Ozawa, K. Itoh, M. Mizugaki, *J. Biochem.* **2001**, *129*, 13 – 27.
[21] S. Noguchi, Y. Nishimura, Y. Hirota, S. Nishimura, *J. Biol. Chem.* **1982**, *257*, 6544 – 6550.
[22] J. M. Durand, N. Okada, T. Tobe, M. Watarai, I. Fukuda, T. Suzuki, N. Nakata, K. Komatsu, M. Yoshikawa, C. Sasakawa, *J. Bacteriol.* **1994**, *176*, 4627 – 4634.
[23] J. M. Durand, B. Dagberg, B. E. Uhlin, G. R. Björk, *Mol. Microbiol.* **2000**, *35*, 924 – 935.
[24] R. Brenk, L. Naerum, U. Grädler, H. D. Gerber, G. A. Garcia, K. Reuter, M. T. Stubbs, G. Klebe, *J. Med. Chem.* **2003**, *46*, 1133 – 1143.
[25] R. Brenk, H.-D. Gerber, J. D. Kittendorf, G. A. Garcia, K. Reuter, G. Klebe, *Helv. Chim. Acta* **2003**, *86*, 1432 – 1452.
[26] E. A. Meyer, R. Brenk, R. K. Castellano, M. Furler, G. Klebe, F. Diederich, *Chembiochem* **2002**, *3*, 250 – 253.
[27] U. Grädler, H. D. Gerber, D. M. Goodenough-Lashua, G. A. Garcia, R. Ficner, K. Reuter, M. T. Stubbs, G. Klebe, *J. Mol. Biol.* **2001**, *306*, 455 – 467.
[28] G. C. Hoops, L. B. Townsend, G. A. Garcia, *Biochemistry* **1995**, *34*, 15 381 – 15 387.

[29] A. Bairoch, R. Apweiler, *Nucleic Acids Res.* **2000**, *28*, 45 – 48.
[30] U. Grädler, PhD thesis, Philipps-Universität Marburg, Germany.
[31] K. Reuter, R. Ficner, *J. Bacteriol.* **1995**, *177*, 5284 – 5288.
[32] G. C. Hoops, J. Park, G. A. Garcia, L. B. Townsend, *J. Heterocyclic Chem.* **1996**, *33*, 767 – 781.
[33] R. M. C. Dawson, D. C. Elliott, W. H. Elliot, K. M. Jones, *Data for Biochemical Research*; 3rd ed., Oxford University press, Oxford, **1969**.
[34] H. J. Böhm, *J. Comput. Aided Mol. Des.* **1992**, *6*, 61 – 78.
[35] C. Romier, R. Ficner, K. Reuter, D. Suck, *Proteins* **1996**, *24*, 516 – 519.
[36] A. W. Curnow, F. L. Kung, K. A. Koch, G. A. Garcia, *Biochemistry* **1993**, *32*, 5239 – 5246.
[37] C. Papworth, J. Braman, D. A. Wright, *Strategies* **1996**, *9*, 3 – 4.
[38] H. Akimoto, E. Imamiya, T. Hitaka, H. Nomura, Nishimura, *J. Chem. Soc. Perkin Trans.* **1988**, *1*, 1638 – 1644.
[39] M. T. Migawa, J. M. Hinkley, G. C. Hoops, L. B. Townsend, *Synth.Commun.* **1996**, *26*, 3317 – 3322.
[40] Z. Otwinowski, W. Minor, *Methods Enzymol.* **1977**, *276 A*, 307 – 326.
[41] A. T. Brünger, P. D. Adams, G. M. Clore, W. L. DeLano, P. Gros, R. W. Grosse-Kunstleve, J. S. Jiang, J. Kuszewski, M. Nilges, N. S. Pannu, R. J. Read, L. M. Rice, T. Simonson, G. L. Warren, *Acta Crystallogr., Sect. D* **1998**, *54*, 905 – 921.
[42] T. A. Jones, J. Y. Zou, S. W. Cowan, M. Kjeldgaard, *Acta Crystallogr. Sect. A* **1991**, *47*, 110 – 119.
[43] J. Navaza, *Acta Crystallogr. Sect. D* **2001**, *57*, 1367 – 1372.
[44] C. S. Bond, *Bioinformatics* **2003**, *19*, 311 – 312.
[45] L. D. Warren, *The PyMOL Molecular Graphics System*, DeLano Scientific, San Carlos, CA, USA, http://www.pymol.org.
[46] A. T. Brünger, *Nature* **1992**, *355*, 472 – 474.

Received: April 30, 2003 [F 644]

